PAPER

Decoupling Network Comprising Transmission Lines and Bridge Resistance for Two-Element Array Antenna

Shumo LI[†a)], ***Student Member and*** **Naoki HONMA**[†], ***Member***

SUMMARY This paper presents a novel decoupling network consisting of transmission lines and a bridge resistance for a two-element array antenna and evaluates its performance through simulations and measurements. To decouple the antennas, the phase of the mutual admittance between the antenna ports is rotated by using the transmission lines, and a pure resistance working as a bridge resistance is inserted between the two antenna ports to cancel the mutual coupling. The simulation results indicate that the proposed decoupling network can provide a wider bandwidth than the conventional approach. The proposed decoupling network is implemented and tested as a demonstration to confirm its performance. The measurement results indicate that the mutual coupling between the two antenna ports is lowered by about 47 dB at the resonant frequency.

key words: *decoupling network, mutual coupling, transmission lines, bridge resistance, array antenna*

1. Introduction

Demand has been growing for the next-generation wireless communication system to offer high-speed transmission within the limited frequency resources. On the other hand, the space for the base-station antennas is limited, too, and sharing antenna space among several wireless systems is required. For such reason, several antennas need to be located immediately adjacent to each other. In this case, the transmitted signal from one wireless system interferes with another one because of the high mutual coupling between the antennas even when their frequency bands are different [1]. Since mutual coupling between the antennas becomes high when the multiple antennas are closely spaced, the communication performance is degraded. Also, when performing power transmission and signal reception simultaneously in wireless power transmission systems, the strong transmitted signal leaks into the receiving antenna due to the mutual coupling between the transmitting and receiving antennas; this saturates the receiver and degrades communication performance. Therefore, high isolation over a broad band is required between the antenna elements.

The most common approach to reducing the effects of mutual coupling is to use a decoupling network (DN). Many studies on DN have been published [2]–[11]. As indicated in [3], although a conventional decoupling and matching network (DMN) is effective in suppressing the mutual coupling between the antenna elements, the configuration of the circuit is complex and its bandwidth is narrow. A DN design that uses a microstrip line (MSL) as the susceptance has been proposed; it offers a simple circuit configuration [4]. However, if the mutual coupling between the antenna elements is small, the MSL must have such high impedance that it cannot be realized since the line width would be narrower than the fabrication limit. The work [5] also presents a design method of a simple decoupling and matching feeding network (DMFN) using transmission lines and bridge susceptances. Only the design formulas of the DMFN have been derived, and how much the bandwidth can be obtained by using this method has been not studied. As described above, a simple DN that is easy to realize and can suppress the mutual coupling over a wide bandwidth is needed.

This paper proposes a novel DN comprising transmission lines and a bridge resistance for a two-element array antenna. The DN uses the transmission lines to realize phase rotation and so address antenna mutual admittance while the bridge resistance obtains the decoupling effect [12], [13]. The result is excellent decoupling characteristics over a relatively wide bandwidth, even when antenna element spacing is tight.

The next section describes the theory of the proposal. The proposal is subjected to simulations and experiments to confirm its wide bandwidth characteristics and its effectiveness.

2. Proposed Circuit Design

2.1 Proposed Decoupling Network Configuration

Figure 1 shows the configuration of the proposed DN. Here, $\boldsymbol{Y}_a$ is the admittance matrix of the antenna. $\boldsymbol{Y}_f$ is the admittance matrix of the transmission lines used to tune the phase of the mutual admittance of the antennas. The length and characteristic impedance of these lines are defined as l_f and Z_f, respectively. As shown in Fig. 1(a), a pure resistance, R, is inserted as a bridge resistance. Since the two antenna elements are spatially separated, the two bridge MSLs with characteristic impedance Z_0 are used to connect the bridge resistance. When the bridge MSLs have line lengths of $\lambda_g/2$ (λ_g: effective wavelength), the equivalent model of the bridge circuit is simplified to a purely resistive element. The admittance matrix of the bridge circuit comprising the MSLs and resistance is defined as $\boldsymbol{Y}_d$. Figure 1(b) shows an equivalent circuit of the DN. The details of the derivation procedure of Figs. 1(b) from (a) will be described in the

Manuscript received October 25, 2013.
Manuscript revised February 20, 2014.

[†]The authors are with the Graduate School of Engineering, Iwate University, Morioka-shi, 020-8551 Japan.
a) E-mail: t2312034@iwate-u.ac.jp

DOI: 10.1587/transcom.E97.B.1395

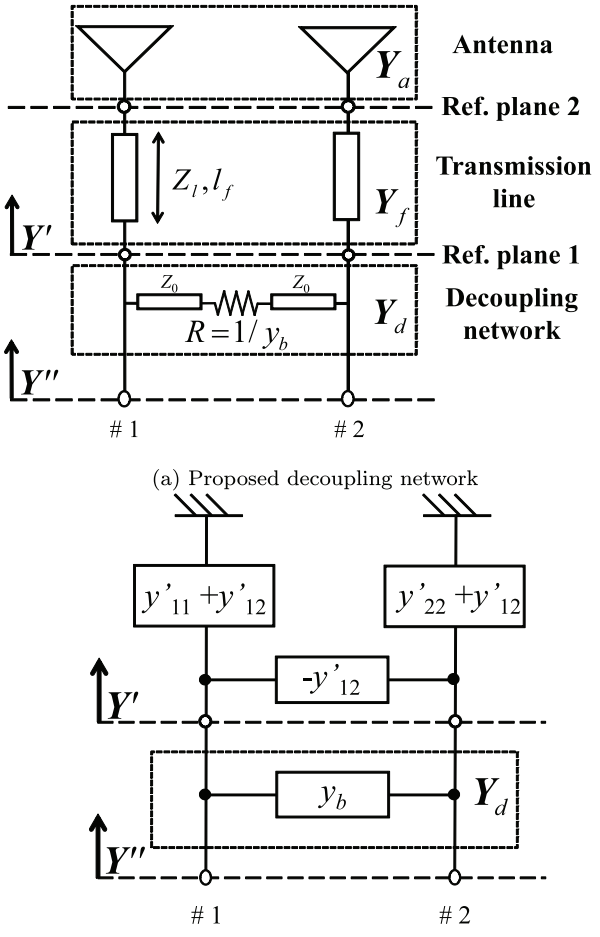

Fig. 1 Proposed decoupling network model.

next Sect. 2.2. In Fig. 1(b), y'_{12} is the mutual admittance; it represents the mutual coupling between the antennas. When $y_b = y'_{12}$, the mutual admittance between feeding port 1 and port 2 would be zero which cancels mutual coupling completely. Since $R = 1/y_b$, y'_{12} must be real positive value to be successfully cancelled by the bridge resistance. Therefore, the length, l_f, of the MSL for phase rotation is determined so as to transform y'_{12} into a real positive value.

2.2 Theory for Circuit Design

A method of deriving circuit design values is described. First, the admittance matrix of the antennas, $\boldsymbol{Y}_a$, is evaluated. Then the MSL length, l_f, and the resistance value, R, are calculated by using the following formula. The admittance matrix of the MSL for phase rotation, $\boldsymbol{Y}_f$, is split into four partitioned matrices as

$$\boldsymbol{Y}_f = \begin{pmatrix} \boldsymbol{Y}_{f11} & \boldsymbol{Y}_{f12} \\ \boldsymbol{Y}_{f21} & \boldsymbol{Y}_{f22} \end{pmatrix}, \tag{1}$$

where the subscript numbers represent the reference planes shown in Fig. 1(a). When $\boldsymbol{Y}_f$ is connected to $\boldsymbol{Y}_a$, the observed admittance matrix at the end of the phase rotation MSL is obtained as

$$\boldsymbol{Y}' = \boldsymbol{Y}_{f11} - \boldsymbol{Y}_{f12}(\boldsymbol{Y}_a + \boldsymbol{Y}_{f22})^{-1}\boldsymbol{Y}_{f21}. \tag{2}$$

For lossless transmission lines, $\boldsymbol{Y}_f$, is determined by the line length, l_f, and the characteristic admittance, Y_f. Additionally, $\boldsymbol{Y}_{f11}$, $\boldsymbol{Y}_{f12}$, $\boldsymbol{Y}_{f21}$, $\boldsymbol{Y}_{f22}$ are given by

$$\boldsymbol{Y}_{f11} = \boldsymbol{Y}_{f22} = -\begin{pmatrix} jY_f \cot\beta l_f & 0 \\ 0 & jY_f \cot\beta l_f \end{pmatrix} \tag{3}$$

$$\boldsymbol{Y}_{f12} = \boldsymbol{Y}_{f21} = \begin{pmatrix} jY_f \csc\beta l_f & 0 \\ 0 & jY_f \csc\beta l_f \end{pmatrix}, \tag{4}$$

where β is wave number in the phase rotation MSL. By expanding (2), the MSL length, l_f, which makes the imaginary part of y'_{21} (y'_{21} is the off-diagonal elements of (2)) zero, is obtained by

$$l_f = \frac{1}{\beta}\tan^{-1}\left(\frac{2A}{-B \pm \sqrt{B^2 - 4AC}}\right). \tag{5}$$

Here, A, B, and C are described as

$$\begin{aligned} A &= Y_f^2 y_{a12i} \\ B &= -Y_f[y_{a12r}(y_{a11r} + y_{a22r}) + y_{a12i}(y_{a11i} + y_{a22i})] \\ C &= y_{a12r}(y_{a11r}y_{a22i} + y_{a22r}y_{a11i} - y_{a12r}y_{a21i}) \\ &\quad - y_{a12i}(y_{a11r}y_{a22r} - y_{a11i}y_{a22i} + y_{a12i}y_{a21i}), \end{aligned} \tag{6}$$

where y_{a11r}, y_{a12r}, y_{a21r}, y_{a22r} are the real part of each element of $\boldsymbol{Y}_a$, and y_{a11i}, y_{a12i}, y_{a21i}, y_{a22i} are the imaginary part of each element of $\boldsymbol{Y}_a$, respectively. At this time, the resistance value, R, is obtained from $R = 1/y'_{21}$. The bridge resistance is connected between the antennas to achieve decoupling, so the admittance matrix of the DN is represented by

$$\boldsymbol{Y}_d = \begin{pmatrix} y_b & -y_b \\ -y_b & y_b \end{pmatrix} = \begin{pmatrix} 1/R & -1/R \\ -1/R & 1/R \end{pmatrix}. \tag{7}$$

Since the DN is connected in parallel to the antennas, the observed admittance matrix $\boldsymbol{Y}''$ with decoupling is denoted as

$$\boldsymbol{Y}'' = \boldsymbol{Y}' + \boldsymbol{Y}_d. \tag{8}$$

From (8), it can be seen that decoupling is realized because the off-diagonal elements of $\boldsymbol{Y}''$ are zero.

3. Simulation

3.1 Simulation Conditions

To confirm that the proposed DN offers wide bandwidth, we simulated the decoupling circuit characteristics and compared to DN with the capacitance instead of the resistance. Here, the DN with capacitance is achieved by replacing the resistance to capacitance in Fig. 1, and the MSL length, l_f, is determined so as that the real part of y'_{21} becomes zero. This section starts be describing the simulation conditions. Figure 2 shows the simulated model of the two basic antennas.

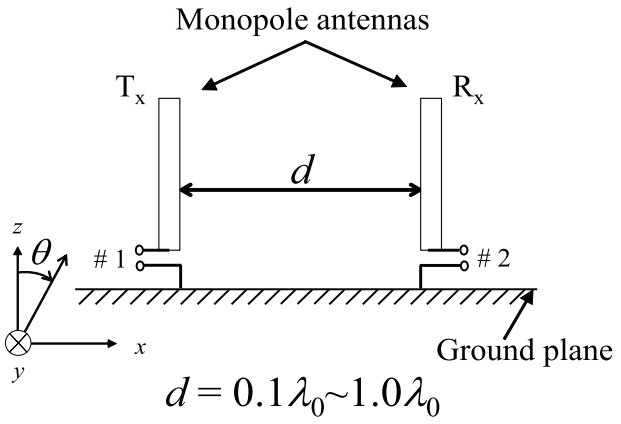

Fig. 2 Simulated model of antennas.

In this study, both antennas are monopoles with resonant frequency of 2.4 GHz. The element spacing, d, between the antennas is varied by 0.1 λ_0 (λ_0: wavelength in vacuum) from 0.1 λ_0 to 1.0 λ_0. The circuit characteristics are evaluated for each element spacing.

3.2 Simulation Results

Figure 3 plots simulated S-parameters versus the element spacing between the antennas at the resonant frequency. Here, the resonant frequency is defined as the frequency where the reflection, S_{11}, of the element alone becomes minimum. Since S-parameter is symmetric in this model, only reflection, S_{11}, and mutual coupling, S_{21}, are shown. In addition, the coupling characteristics without DN and the simulated DN with capacitance are also shown here. Figure 3(a) confirms that the reflection characteristic, S_{11}, of decoupling with capacitance is the same as that with resistance. The reflection characteristics of the antenna itself are between −10 dB and −25 dB, and the reflection characteristics of the antenna with DN are between −10 dB to −20 dB, too. Although the reflection level, S_{11}, with DN is higher than that without DN, there is no significant effect of DN on the antenna performance since S_{11} is still lower than −10 dB with various d. The degradation in S_{11} with decoupling is thought to be due to the addition of the diagonal elements of $\boldsymbol{Y}_d$ that cause changes in self-admittance and the effect on the reflection coefficient. In Fig. 3(b), the mutual coupling, S_{21}, is simply reduced as antenna element spacing, d, is increased. Here, only the raw S_{21} value without DN is shown since S_{21} with DN is always 0. This result shows that the proposed DN yields high isolation between the antennas regardless of antenna element spacing. Also, from this result, it can be seen that mutual coupling still remains even with the increase of the distance between the antennas. This can be said that the DN is certainly needed to obtain high isolation of the antennas even if the antenna element spacing is increased.

Figures 4(a) and (b) show the frequency characteristics of mutual coupling, S_{21}, for the antenna element spacing of 0.2 λ_0 and 0.8 λ_0, respectively. The cases with resistance

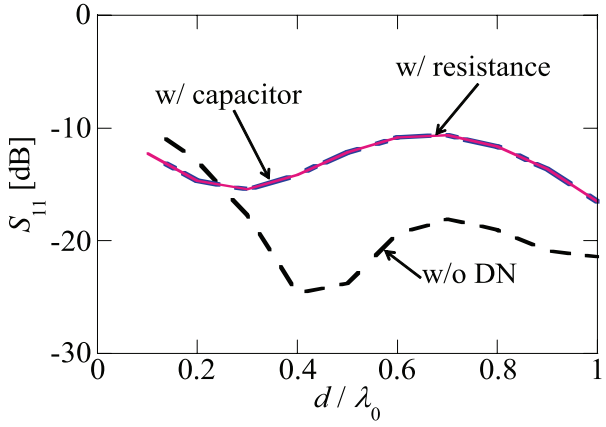

(a) Reflection characteristics S_{11} versus antenna element spacing

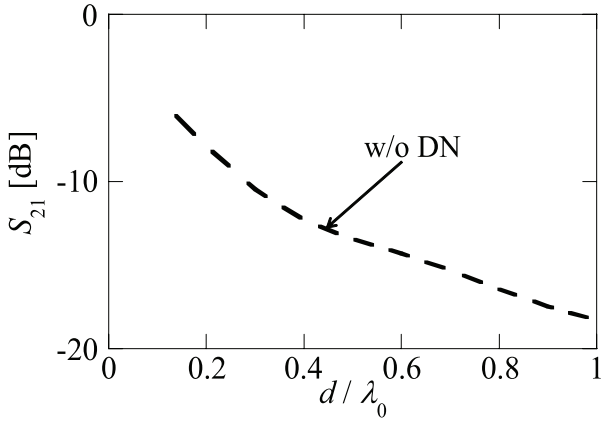

(b) Mutual coupling S_{21} versus antenna element spacing

Fig. 3 S-parameters versus antenna element spacing.

and capacitance were simulated. From Figs. 4(a) and (b), it can be seen that the mutual coupling, S_{21}, were successfully lowered by DNs with both capacitance and resistance regardless of the antenna element spacing, d. Also, it can be seen that the DN with resistance suppresses the mutual coupling, S_{21}, over the wide band of 2.1 GHz~2.7 GHz when d = 0.2 λ_0. On the other hand, it is found that the decoupling bandwidth for the DNs with the resistance and capacitance is almost identical when d = 0.8 λ_0.

Figure 5 shows the fractional bandwidth versus antenna element spacing between the antennas. The bandwidth is defined as a frequency range where the mutual coupling is lower than a certain value. The evaluation of the −20 dB bandwidth versus antenna element spacing is shown in Fig. 5(a) and the evaluation of the −30 dB bandwidth versus antenna element spacing is shown in Fig. 5(b). For comparison, the results gained when using the capacitance are also shown. Figure 5 shows that when the antenna element spacing is narrower than 0.7 λ_0, using the resistance yields relatively wider available bandwidth than using the capacitance. This result indicates that the proposed decoupling design is effective, especially when the antenna element spac-

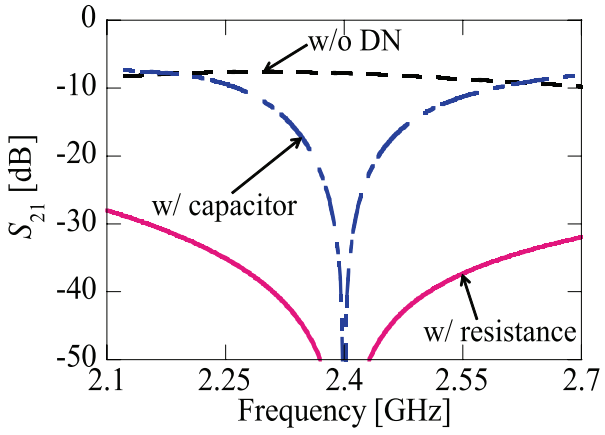

(a) $d = 0.2\ \lambda_0$

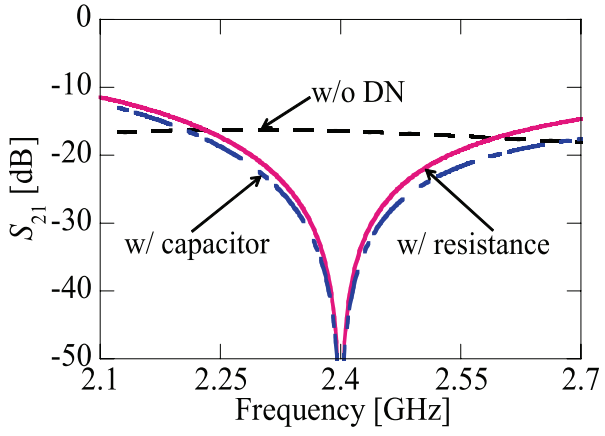

(b) $d = 0.8\ \lambda_0$

Fig. 4 Frequency characteristics of mutual coupling S_{21}.

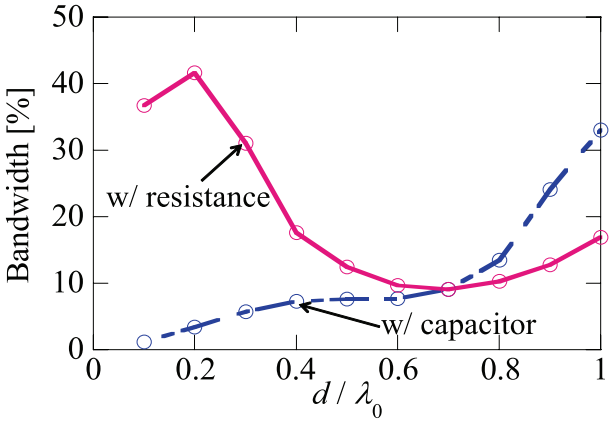

(a) −20 dB bandwidth versus antenna element spacing

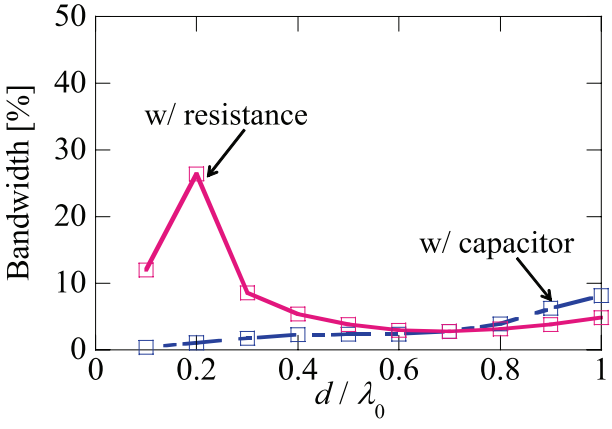

(b) −30 dB bandwidth versus antenna element spacing

Fig. 5 Fractional bandwidth versus antenna element spacing.

ing becomes narrow.

Figures 6(a) and (b) show the frequency characteristics of real and imaginary parts of the mutual admittance, y'_{21}, respectively. Here, the mutual admittance is observed at the reference plane 1 shown in Fig. 1(a). Note that the line lengths, l_f, in DNs with resistance and capacitance are different since the required degree of the phase rotation is different for these two DNs. The antenna element spacing was set to $d = 0.2\ \lambda_0$, $0.5\ \lambda_0$, $0.7\ \lambda_0$, and $1.0\ \lambda_0$ as an example. Figure 6(b) shows that the curves for DN with capacitance are steeper than that with resistance when the antenna spacing is narrow. Since y'_{21} and the bridge admittance, y_b, should be cancelled out each other, the rapid change yields narrow bandwidth of DN. Therefore, the bandwidth of the DN with capacitance becomes narrow in this case. On the contrary, the curves for DN with resistance in Figs. 6(a) and (b) are almost constant when $d = 0.2\ \lambda_0$, and this means the wide decoupling bandwidth is expected since y'_{21} and y_b cancel out each other over the wide range. However, the spectral fluctuation of the mutual admittance, y'_{21}, of DN with the resistance becomes large when $d > 0.7\ \lambda_0$. This affects the bandwidth of the decoupling characteristics. For the above reason, the DN with resistance loses the advantage in bandwidth when $d \geq 0.7\ \lambda_0$.

Adding a resistance to the circuit generally increases the insertion loss, which cannot be ignored. Figure 7 plots the radiation efficiency of the DN with resistance and with capacitance versus the antenna element spacing. The result without DN is also shown. From Fig. 7, it can be confirmed that the radiation efficiency of the DN with capacitance is close to 100 percent regardless of the antenna element spacing. However, while the radiation efficiency of the DN with resistance increases with antenna element spacing, it is always lower than that with capacitance. This result shows that the radiation efficiency of the proposed DN is reduced if the resistance is used. Additionally, it can also be seen that compared to the result without DN, the radiation efficiency of DN with capacitance falls as the antenna element spacing exceeds $0.5\ \lambda_0$. This is because the radiation efficiency also includes the reflection loss of the circuit.

Figure 8 shows the S-parameter model of the antenna and DN. In Fig. 8, $\boldsymbol{a}_1$,$\boldsymbol{a}_2$ are the waves incident to the DN, and $\boldsymbol{b}_1$,$\boldsymbol{b}_2$ are the waves reflected from the DN. The insertion loss of the DN is calculated by

$$\text{Loss} = 10\log_{10}\left(\frac{P_{\text{out}}}{P_{\text{in}}}\right). \tag{9}$$

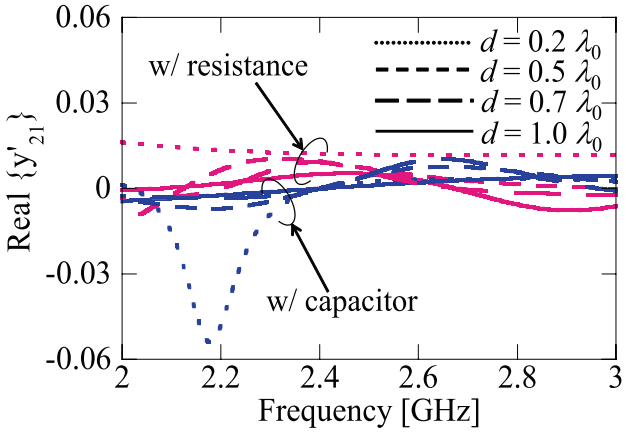

(a) Real part of y'_{21}

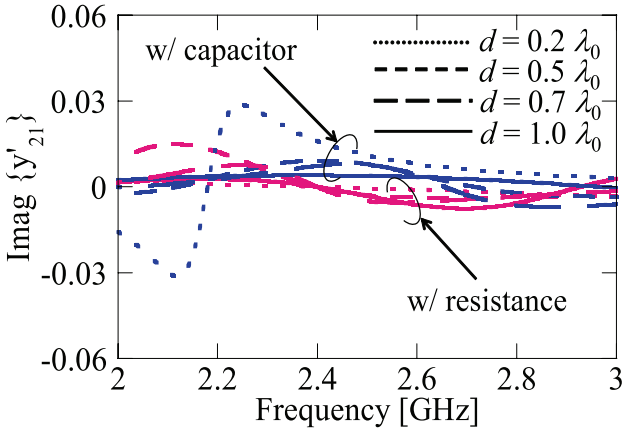

(b) Imaginary part of y'_{21}

Fig. 6 Frenquency characteristics of mutual admittance, y'_{21}.

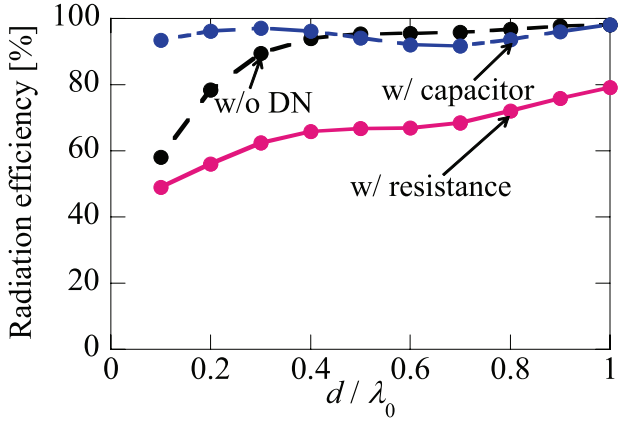

Fig. 7 Radiation efficiency versus antenna element spacing.

Here, P_{in} is the input power to the DN, P_{out} is the input power to the antennas; they are defined by

$$P_{\text{in}} = |\boldsymbol{a}_1|^2 - |\boldsymbol{b}_1|^2$$
$$P_{\text{out}} = |\boldsymbol{b}_2|^2 - |\boldsymbol{a}_2|^2. \quad (10)$$

Figure 9 shows the insertion losses of the proposed

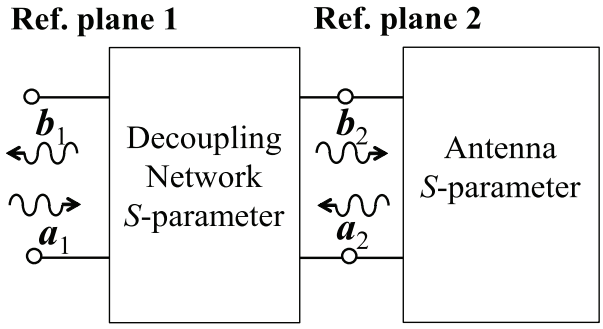

Fig. 8 S-parameter model of antenna and DN.

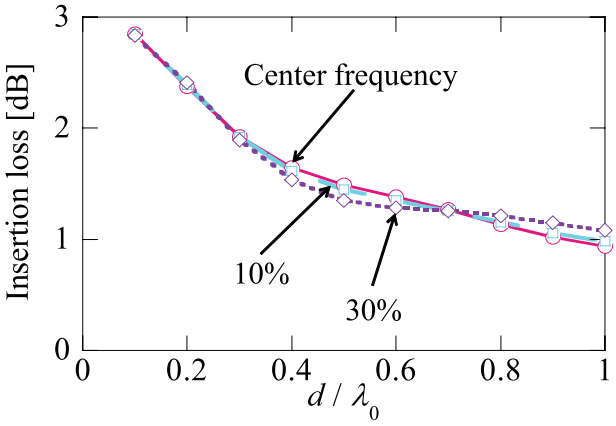

Fig. 9 Insertion losses versus antenna element spacing.

DN versus the antenna element spacing. Here, the bridge resistance values were determined to suit the resonant frequency, 2.4 GHz. When the frequency range is defined as 2.1 GHz~2.7 GHz temporarily, the results of the insertion loss at a frequency of 10 percent and 30 percent value of the bandwidth are also presented. From Fig. 9, it can be found that the circuit loss is large when the antenna element spacing is narrow if either at the resonant frequency or not. The maximum circuit loss at any frequency indicated, under 3 dB, occurs at the narrowest antenna element spacing, $d = 0.1\ \lambda_0$.

Figure 10 shows the impact of DN with resistance and with capacitance on the xy-plane radiation pattern. Here, the xy-plane radiation pattern is shown as the actual gain; the results without DN are also shown. Since the antenna structure is symmetric, only the radiation patterns when feeding port 1 are shown. (a), (b), and (c) are for the antenna element spacing values of $d = 0.2\ \lambda_0$, $d = 0.5\ \lambda_0$, $d = 0.8\ \lambda_0$, respectively. By comparing the results with and without DN, it can be seen that there is no significant change in the radiation patterns and gain with either resistance or capacitance. In addition to that, compared the results with DN using the resistance and capacitance, the effect on the antenna gain is much larger when the proposed DN is used. This is caused by the circuit loss of the proposed DN using the resistance.

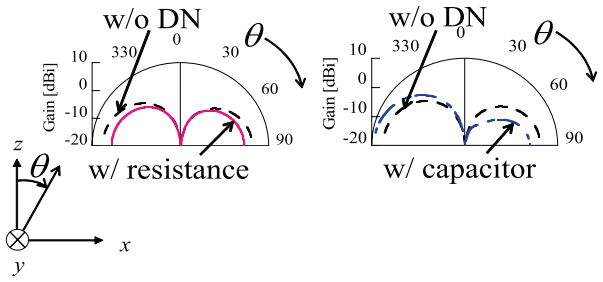

(a) $d = 0.2\ \lambda_0$ (Feeding port ♯ 1)

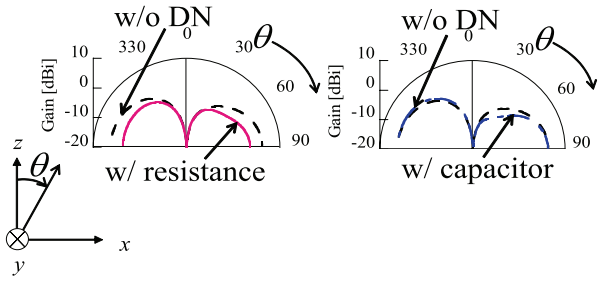

(b) $d = 0.5\ \lambda_0$ (Feeding port ♯ 1)

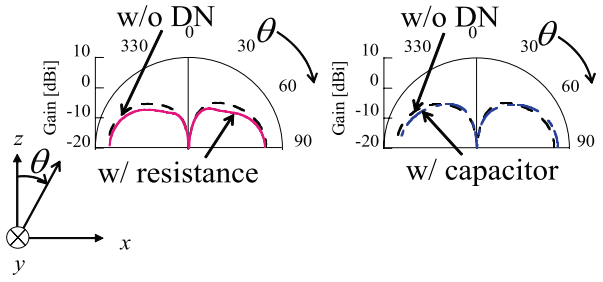

(c) $d = 0.8\ \lambda_0$ (Feeding port ♯ 1)

Fig. 10 Impact of decoupling network on radiation pattern.

4. Experimental Demonstration

4.1 Design of Fabricated Circuit

In this section, the decoupling effect of the proposed circuit design method is demonstrated by measurements on a two-element monopole array antenna following the simulation setup. Figure 11 shows the photo of the measurement setup. The antenna element spacing, d, is 0.5 λ_0, i.e., $d = 62.5$ mm.

Figure 12 shows the monopole antenna configuration designed for this experimental demonstration. The rectangle aluminum plate, whose dimensions are $W_x \times W_y = 300 \times 300\ \text{mm}^2$, is used as a finite ground plane of the two-element monopole antenna. The monopole antennas are configured symmetrically on the ground plate and are cylindrical conductor whose dimensions are given as $L = 28.9$ mm and $a = 3$ mm. The resonant frequency of the antennas is in the vicinity of 2.4 GHz.

Figure 13(a) shows the design of the proposed DN

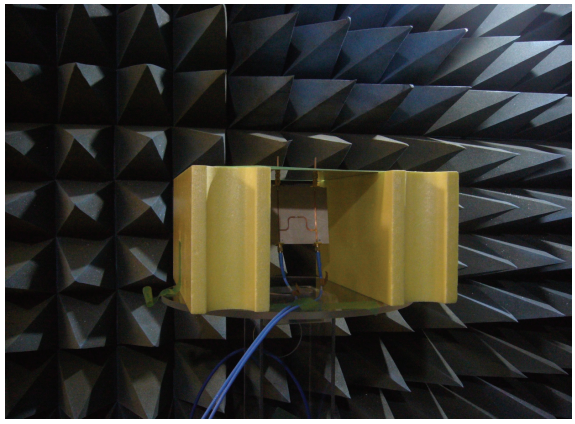

Fig. 11 Measurement setup.

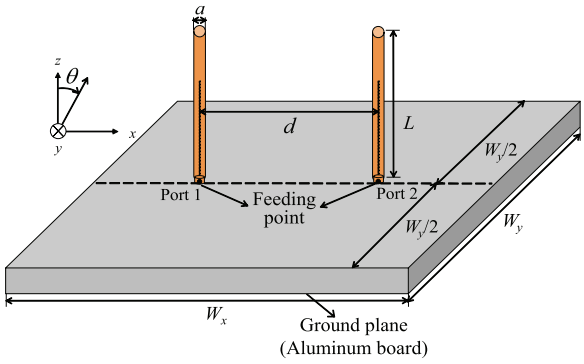

Fig. 12 Configuration of monopole antennas.

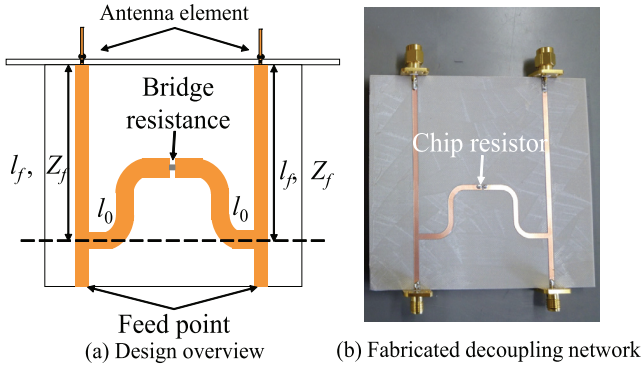

(a) Design overview (b) Fabricated decoupling network

Fig. 13 Design for proposed decoupling network.

based on measured values of the antenna elements. The values of line length, l_f, of the MSL for phase rotation and the bridge resistance, R, were calculated by using the derivation method mentioned in Sect. 2. Here, $l_f = 73.1$ mm and $R = 113.4\,\Omega$. Figure 13(b) is a photo of the fabricated DN. The line length of the two bridge MSLs is $l_0 = 45.8$ mm. The two MSLs are bent to fit within the antenna element spacing since total MSL length is greater than the element spacing of the antenna. The bridge resistance was realized as a chip resistor with $R = 110.1\,\Omega$; this value is only slightly different from the desired value.

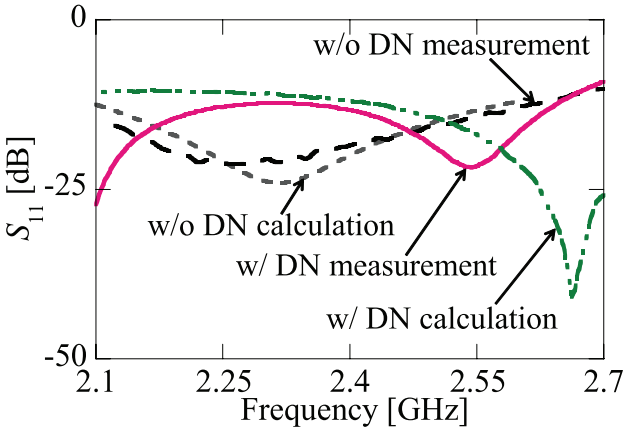

(a) Frequency characteristics of reflection characteristic S_{11}

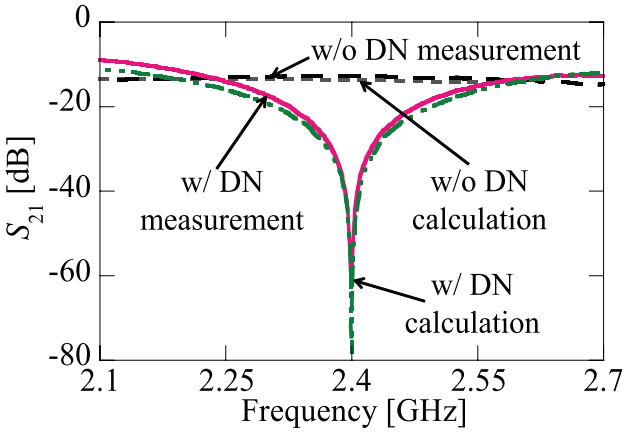

(b) Frequency characteristics of mutual coupling S_{21}

Fig. 14 Frequency characteristics of S-parameters.

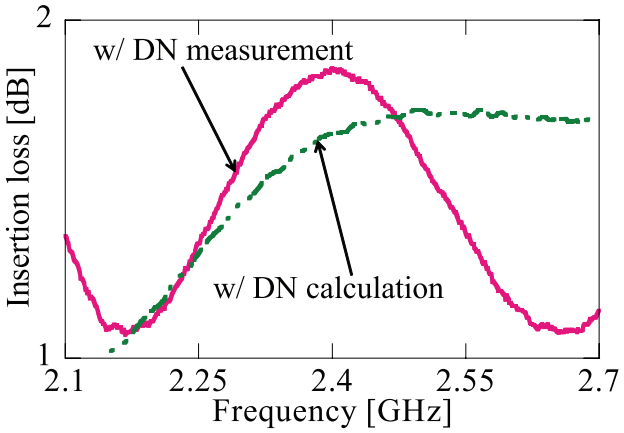

Fig. 15 Frequency characteristics of insertion loss.

4.2 Measurement Results

Figure 14 shows the frequency characteristics of the measured S-parameters. Here, the simulated DN and the coupling characteristics without the DN on simulation and experiment were also shown. It should be noted that the simulation results shown here were calculated by the measured values of the antennas and the design values of the DN. The self-admittance after decoupling is changed by using the resistance, and this can alter the reflection coefficient. Because of this, both the simulated and the measured S_{11} after decoupling are changed in Fig. 14(a). Comparing the simulated and the measured S_{11}, it can be seen the resonant frequency is shifted. The reason of this can be considered to be due to the inclusion of the imaginary component in the chip resistor used in the measurement system. From Fig. 14(b), it can be seen that simulated and measured S_{21} values after decoupling generally agree. Also, it can be seen that the operation frequency is the same as the resonant frequency and the mutual coupling, S_{21}, can be suppressed by about 47 dB at maximum.

Figure 15 shows the frequency characteristics of the insertion loss when using the proposed DN; the simulated result is also shown. From this figure, it can be found that the circuit loss due to the resistance is below 2 dB in both the simulation and the experiment. Furthermore, the results of circuit loss shown in Fig. 9 and Fig. 15 are compared with at the resonant frequency, 2.4 GHz. The simulated circuit loss shown in Fig. 9 at 2.4 GHz is about 1.5 dB, the circuit loss by calculation and measurement shown in Fig. 15 at 2.4 GHz are about 1.51 dB and 1.86 dB, respectively. These results show that there is no significant difference between the simulated and measured losses. According to the simulation described in Sect. 3, the radiation efficiency is mainly determined by the DN since the radiation efficiency of the antenna elements except for the reflection and the circuit loss is approximately 100 percent. Similarly, it is estimated that the radiation efficiency of the antennas with proposed DN would be around 65 percent on the basis of the circuit loss in experiment.

Figures 16(a) and (b) show the measured and simulated radiation patterns for port 1 and 2, respectively, for DN and without DN. The radiation patterns are shown in the actual gain where the reflection and the circuit losses are considered. Figure 16 confirms that the measured and simulated radiation patterns are in quite good agreement. Since the measured patterns and gain show no significant change after decoupling, it can be said that the circuit loss of the proposed DN has small impact on the radiation pattern and efficiency of antenna.

5. Conclusion

This paper proposed a decoupling network comprising transmission lines and bridge resistance for a two-element array antenna. MSLs for phase rotation are connected in series to the antennas to transform the phase of the mutual admittance, and the decoupling effect is realized by connecting a bridge resistance in parallel between the antennas. Simulations of the monopole array antennas showed that the proposed DN using the resistance can obtain a wider bandwidth as compared to the DN using a capacitance when the antenna element spacing is narrower than 0.7 λ_0. Moreover, experiments showed that the mutual coupling is improved

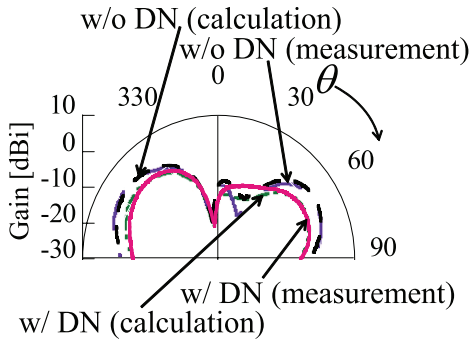

(a) Feeding port ♯1

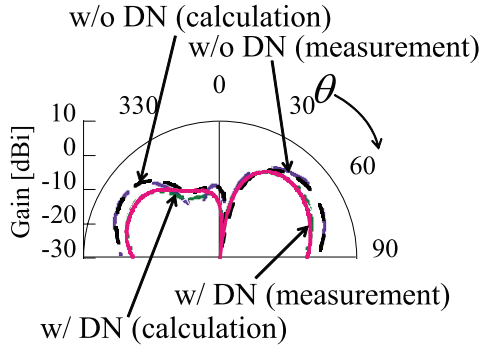

(b) Feeding port ♯2

Fig. 16 Radiation patterns ($d = 0.5\lambda_0$).

by about 47 dB at the resonant frequency without serious degradation in the gain of the radiation patterns. These results prove that the proposed decoupling network is effective in suppressing the mutual coupling over a broad bandwidth even if the element spacing is narrow.

Acknowledgements

This research was partially supported by JSPS KAKENHI (25709030).

References

[1] A. Kishida, T. Hiraguri, M. Ogawa, K. Nishimori, N. Honma, and T. Sakata, "A novel interference avoidance technique on mobile wireless routers using IEEE802.11nPSMP," IEICE Trans. Commun., vol.E93-B, no.8, pp.2053–2062, Aug. 2010.

[2] J.B. Andersen and H.H. Rasmussen, "Decoupling and descattering networks for antennas," IEEE Trans. Antennas Propag., vol.AP-24, no.6, pp.841–846, Nov. 1976.

[3] J. Weber, C. Volmer, K. Blau, R. Stephan, and M.A. Hein, "Miniaturized antenna arrays using decoupling networks with realistic elements," IEEE Trans. Wicrow. Theory Tech., vol.54, no.6, pp.2733–2740, June 2006.

[4] N. Yamaki and N. Honma, "Decoupling technique for n-element linear array antenna using transmission lines between neighboring elements," IEICE Communications Express, vol.1, no.7, pp.246–251, Dec. 2012.

[5] K. Kagoshima, S. Obote, A. Kagaya, K. Nishimura, and N. Endo, "An array antenna for MIMO systems with decoupling network using bridge susceptances," 2011 Wireless VITAE, 2011.

[6] S.C. Chen, Y.S. Wang, and S.J. Chung, "A decoupling technique for increasing the port isolation between two strongly coupled antennas," IEEE Trans. Antennas Propag., vol.56, no.12, pp.3650–3658, Dec. 2008.

[7] A.C.K. Mak, C.R. Rowell, and R.D. Murch, "Isolation enhancement between two closely packed antennas," IEEE Trans. Antennas Propag., vol.56, no.11, pp.3411–3419, Nov. 2008.

[8] J.C. Coetzee and Y. Yu, "Port decoupling for small arrays by means of an eigenmode feed network," IEEE Trans. Antennas Propag., vol.56, no.6, pp.1587–1593, June 2008.

[9] J. Itoh, N.T. Hung, and H, Morishita, "The mutual coupling reduction between two j-shaped folded monopole antennas for handset," IEICE Trans. Commun., vol.E94-B, no.5, pp.1161–1167, May 2011.

[10] H. Jiang, R. Yamaguchi, and K. Cho, "Reduction in mutual coupling characteristics of slot-coupled plannar antenna due to rectangular elements," 2008 IEEE Intl. ANt and Prop. Society Symp., 137.7 July 2008.

[11] H. Jiang, R. Yamaguchi, and K. Cho, "Bandwidth characteristic improvement of filter integrated antenna composed of aperture coupled patch antenna by using trapezoidal element," IEICE Trans. Commun., vol.E92-B, no.12, pp.3960–3963, Dec. 2009.

[12] S. Li, N. Honma, and N. Yamaki, "Proposal of tunable decoupling network comprising transmission lines and lumped elements," 2012 International Symposium on Antenna and Propagation (ISAP 2012), Electroc Proc. ISAP 2012, 1E4-2, Oct. 2012.

[13] S. Li, N. Honma, and N. Yamaki, "Decoupling network comprising transmission lines and bridge resistance for two-element array antenna," 2012 Asia Pacific Microwave Conference (APMC2012), 3C4-04, Dec. 2012.

Shumo Li was born in Changchun, Jilin, China, in 1988 and came to Japan for study in 2006. She received the B.E. and M.E. degrees in electrical and electronic engineering from Iwate University, Morioka, Japan in 2012 and 2014, respectively. She joined NTT docomo in 2014. Her research interest is decoupling network which applies to wireless power transmission using array antennas.

Naoki Honma received the B.E., M.E., and Ph.D. degrees in electrical engineering from Tohoku University, Sendai, Japan in 1996, 1998, and 2005, respectively. In 1998, he joined the NTT Radio Communication Systems Laboratories, Nippon Telegraph and Telephone Corporation (NTT), in Japan. He is now associate professor in Iwate University. He is an Associate Editor for the Transactions on Communications for the IEICE Communications Society from May 2011. He received the Young Engineers Award from the IEICE of Japan in 2003, the APMC Best Paper Award in 2003, and Distinguished Service Award from the IEICE Communications Society in 2011. His current research interest is MIMO antenna technology for high-speed wireless communication systems. He is a member of the Institute of Electronics, Information and Communication Engineers (IEICE) of Japan.